frontiers | Frontiers in Earth Science

ORIGINAL RESEARCH
published: 12 July 2022
doi: 10.3389/feart.2022.946437

The Small Strain Stiffness Properties of Undisturbed Weathered Granite With Different Weathering Degrees

Juntao Wang[1,2], *Lingwei Kong*[1,2]*, *Chengsheng Li*[3], *Bingheng Liu*[1,2] and *JunBiao Yan*[1,2]

[1]State Key Laboratory of Geomechanics and Geotechnical Engineering, Institute of Rock and Soil Mechanics, Chinese Academy of Sciences, Wuhan, China, [2]University of Chinese Academy of Sciences, Beijing, China, [3]Department of Civil and Environmental Engineering, Shantou University, Shantou, China

To evaluate the small strain stiffness properties of undisturbed weathered granite, the circular computer numerical control (CNC) abrasive wire sawing technology was applied to weathered granite sample processing and a series of resonance column tests were carried out to study the effects of weathering degree and effective consolidation pressure on dynamic shear modulus of undisturbed weathered granite. The results show that the degree of weathering and effective consolidation pressure have significant effects on the small strain stiffness properties of weathered granite. The samples with lower weathering degrees have higher dynamic shear modulus under the same effective consolidation pressure. The maximum dynamic shear modulus of samples with higher weathering degrees is more sensitive to effective consolidation pressure. Besides, a comparison between the experimental results with the previous results from other researchers indicates that the dynamic shear modulus ratio of weathered granite in the study area exceeds the parameter range obtained from others. According to the experimental results, a mathematical model of the relation between corrected standard penetration test (SPT) *N*' value and dynamic shear modulus was established, and besides, the variation range of dynamic shear modulus ratio of weathered granite in the study area was given, which may provide a reference for dynamic stability analysis of engineering in the study area.

Keywords: weathered granite, resonant column test, dynamic shear modulus, abrasive wire sawing technology, small strain stiffness properties

OPEN ACCESS

Edited by:
Zetian Zhang,
Sichuan University, China

Reviewed by:
Min Wang,
Los Alamos National Laboratory (DOE), United States
Yun Yang,
University of Calgary, Canada

***Correspondence:**
Lingwei Kong
lwkong@whrsm.ac.cn

Specialty section:
This article was submitted to Geohazards and Georisks, a section of the journal Frontiers in Earth Science

Received: *17 May 2022*
Accepted: *22 June 2022*
Published: *12 July 2022*

Citation:
Wang J, Kong L, Li C, Liu B and Yan J (2022) The Small Strain Stiffness Properties of Undisturbed Weathered Granite With Different Weathering Degrees. Front. Earth Sci. 10:946437. doi: 10.3389/feart.2022.946437

INTRODUCTION

Weathered granite is the product of the physical and chemical weathering of intact granite left *in situ* (Irfan, 1996), which is widely distributed in the world. Due to its special genesis, the weathered granite is generally characterized by multiple fractures in structure and is easy to break. The weathered granite particles are irregular in shape with large edges and corners. In addition, the weathered granite is usually weak in cementation and easy to collapse in case of water (Liu et al., 2019). Therefore, the weathered granite is a special geomaterial, whose physical and mechanical properties are different from sedimentary soil and sand. To study the particular property of weathered granite, many studies have been carried out since the 1960s (Lee, 1965). The research emphasis developed from the engineering qualitative classification (Irfan and Dearman, 1978), the basic physical properties (Lee, 1965), and the deformation/strength characteristics (Lee and Coop, 1995) to the hydraulic/mechanical properties of unsaturated weathered granite (Xiong et al., 2022), the microstructure distribution of the intact weathered granite (Shang et al., 2015) and the

relationship between the microstructure and deformation of weathered granite (Li et al., 2020). In addition, the properties of weathered granites were compared with other geomaterials and any fruitful research results provide important new insights for reference. However, the water and mud inrush disasters (Liu et al., 2019) and ambient rock collapse in the tunnel, slope collapse (Zhang et al., 2021), and other problems (Cui et al., 2016) still frequently occurred in the process of engineering construction in weathered granite strata, which caused a large number of economic losses and serious casualties. It should be said that there is still an inadequate systematic and comprehensive cognition of engineering characteristics of weathered granites.

With the development of rock weathering degree, the fissure of weathered granite evolved progressively and the structure developed from a massive texture to a cataclastic structure (Irfan, 1996). Compared with the integral structure of granite rock and fine-grained texture of granite residual soil, the interlocking structure of weathered granites with large particles is easier to be damaged in the probe drilling process for borehole specimens. As a result, the undisturbed weathered granite sample is very difficult to get. In addition, due to the large size and high strength of the unweathered mineral, such as quartz, feldspar, and hornblende, the weathered samples are extremely easy to break in the traditional sample-making process, such as the cutting method. Due to the low success rate of the undisturbed sample preparation, the existing research on the undisturbed lower degree weathered granite still lacks. For highly weathered granite, existing studies mostly involve remodeled samples instead of undisturbed samples (Niu et al., 2014; Niu et al., 2015). However, due to the structural nature of rock and soil materials, the remodeled sample preparation process will destroy the original structure and change the nature of geomaterials (Burland et al., 1996), resulting in the distortion of obtained parameters and certain limitations in the application of the parameters. In addition, due to the difference in mineral composition and genesis of protolith, climate environment, and topographic and geomorphic conditions, the process and production of granite weathering generally have distinctive regional characteristics. As a result, weathered granite in different areas exhibits different characteristics. Currently, studies on weathered granites are concentrated in South and Southeast China (Liu et al., 2019; Liu P. et al., 2021; Liu X. et al., 2021), and the Shandong Peninsula (Wang et al., 2016) in China. Although the application of the research results to engineering construction in other areas has a certain reference value, undesirable effects may indeed occur during the construction.

The shear modulus (G) at small strains is a very important fundamental input parameter in the numerical analysis of geotechnical engineering dynamics (e.g., prediction of soil deformation behavior under earthquake, blasting, mechanical or traffic loading, and soil-structure interaction, etc.), and the reasonableness and reliability of its value has a significant impact on the reasonableness and credibility of the calculation results of dynamic analysis (e.g., soil deformation and soil-structure stability). Several test techniques have been used to study the small strain stiffness of geotechnical materials, including resonant columns (Macari and Hoyos, 1996), blender elements (Ng and Yung, 2008), and seismic tests (Ng and Wang, 2001). The research relative to the dynamic response of geomaterials has been focused mostly on sedimentary soils and sand. Studies thus far have suggested that the small strain stiffness properties are affected by many parameters (e.g., effective consolidation pressure (Niu et al., 2014), void ratio, plasticity, structure (Kong et al., 2017), degree of saturation (Ng and Yung, 2008), stress history (Li et al., 2021), gradation (Huang et al., 2021), and sample disturbance (Macari and Hoyos, 1996)). Macari and Hoyos (1996) studied the effects of weathering degree and remodeling disturbance on the small strain stiffness properties of granite residual soils at different depths in Hong Kong. The results show that the maximum dynamic shear modulus G_{max} increases with depth for undisturbed samples and the influence of remolding is noticeable for granite residual soils, the remolded samples from deeper zones sometimes show higher shear moduli than the undisturbed samples. Niu et al. (2014) investigated the effect of the effective consolidation pressure on G_{max} and damping properties by resonant column tests for the remodeled highly weathered granite. Liu X. et al. (2021) explored the effect of cementation among soil particles on small-strain stiffness properties for undisturbed and remolded granite residual soil samples. In contrast, the small strain stiffness characteristics of undisturbed weathered granites with a low degree of weathering are less studied, especially for weathered granites with different degrees of weathering in the laboratory. However, it is inevitable that weathered granites with different weathered degrees show different small strain stiffness properties due to their different microstructures and soil state (Ng and Wang, 2001).

The objective of this study is to investigate the small strain stiffness properties of undisturbed weathered granite with low weathering degrees by the resonant column test. As far as the authors are aware, the study of weathered granite on small strain stiffness properties is still in the stage of exploration (Niu et al., 2014), and the present study is the first study of the small strain shear modulus of undisturbed weathered granite with low weathering degrees by the resonant column test. Besides, the results of undisturbed weathered granite are compared with that of remodeled weathered granite, residual soils, and other geotechnical materials in other areas. The nonlinear deformation characteristics of completed and highly weathered granites in the study area under a small strain condition were studied and the recommended values of relevant dynamic parameters were given to provide basic scientific data for engineering construction and seismic fortification analysis in the study area.

MATERIALS AND METHODS

Stratigraphic Lithology of Weathered Granites

The samples in this study were collected from the Lincang area. The Lincang area, a border city of Yunnan Province in Southwest China, is located in the southern extension part of the Nushan Mountain range of the Hengduan Mountain system, where the high mountains crisscross. Lincang is an important port city for Yunnan to open to Southeast Asia. Therefore, in the past decade, Lincang has been vigorously developed in infrastructure construction and a large number of high speed railway and expressway projects are under construction or completed construction. Lincang area is located on the Lincang-Menghai Granite batholith (Li, 1996), which is about 350 km long from north to south and 10–48 km wide, with a total area of nearly 8000 km^2. Therefore, the railway and expressway projects in the Lincang area are mostly constructed on weathered granite strata. Due to the special properties of weathered granite, engineering construction in the Lincang area has also encountered a series of engineering problems, such as water inrush and mud gushing disasters (Quan et al., 2021). However, very little is known about a systematical research on the properties of weathered granite in the Lincang area. At the same time, Yunnan Province is located on the eastern edge of the collision zone between the Indian Ocean plate and the Eurasian Plate, which is the most active seismic area in the world and is one of the provinces with the most frequent seismic activities and the most serious earthquake disasters in China. Yunnan Province includes seven seismic belts, and the Lincang area is located on the Lancang-Gengma seismic belt. Earthquakes have occurred frequently in the history of the study area. The largest earthquake recently occurred on 6 November 1988, in the Lancang-Gengma area, which is under the jurisdiction of Lincang, with a magnitude 7.6 earthquake followed by an aftershock of magnitude 7.2 (Yi et al., 2014), causing great economic losses and casualties. Yet, to date, there has been no research specific to the dynamic behavior of weathered granites in the Lincang area. The studied samples were collected from a slope of the M-L Expressway East Interchange project in Linxiang District in Lincang City (latitude 23°915′N, longitude 100°133′E). According to the drilling results, the site stratum map is shown in **Figure 1**, and the stratum distribution from top to bottom is as follows.

1) Stratum 1 is mainly composed of silty clay. The silty clay is mainly composed of clay and powder, containing a small amount of sand. The thickness of this layer is 1–3 m.
2) Stratum 2 is composed of completely weathered granite (CWG). The main mineral composition is feldspar, quartz, and biotite and most minerals decomposed into soil. The completely weathered granite has a granular structure (as shown in **Figure 1**), in which the particle size is medium to fine grain. The original rock structure is destroyed, but still could be recognizable. The thickness of the layer is generally greater than 15 m and locally larger than 25 m.
3) Stratum 3 is composed of highly weathered granite (HWG). The main mineral composition is feldspar, quartz, and biotite and some minerals decomposed into soil. The highly weathered granite is also a granular structure (as shown in **Figure 1**), in which the particle size is medium to fine grain. The original rock structure is violently weathered and basically destroyed but could be recognizable easily. The thickness of the layer is generally 10–20 m.
4) Stratum 4 is composed of moderately weathered granite. The minerals are mainly composed of feldspar, quartz and biotite and other minerals, with few minerals decomposed into soil (as shown in **Figure 1**). The moderately weathered granite is a massive structure, in which the particles are medium-fine grain. The original rock structure is retained basically and could be recognizable easily. The moderately

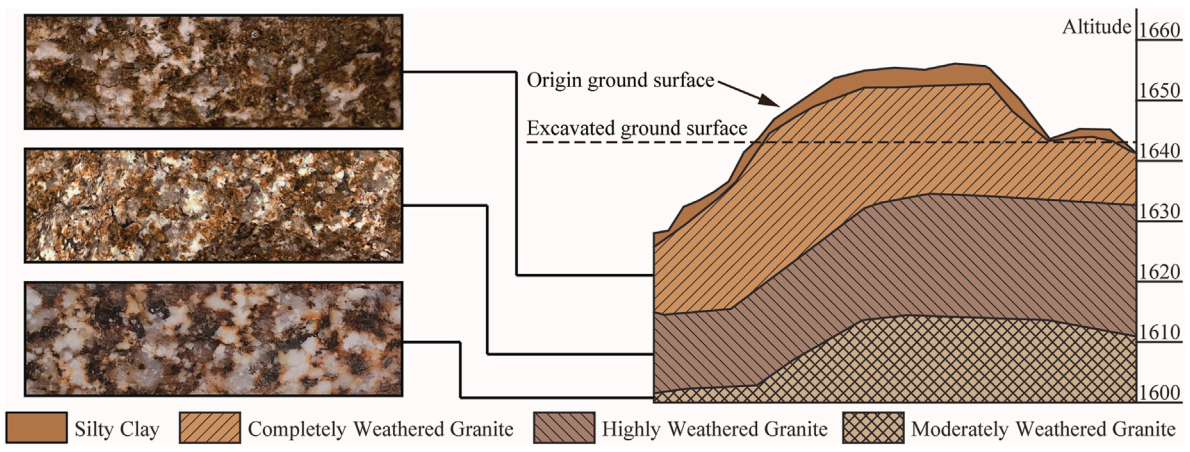

FIGURE 1 | Stratigraphic sections of the research site.

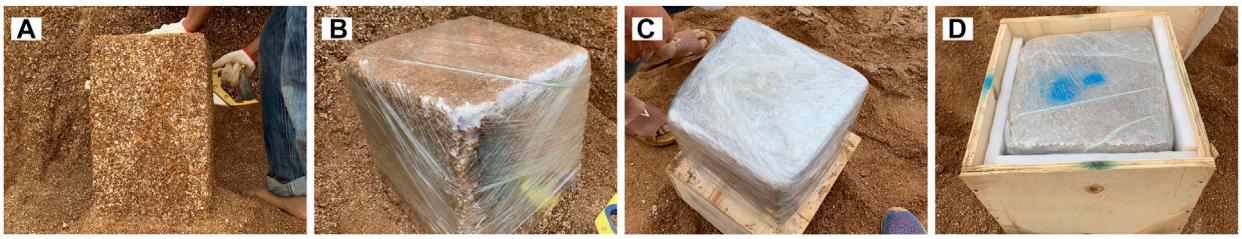

FIGURE 2 | Photos of in-situ sample collection.

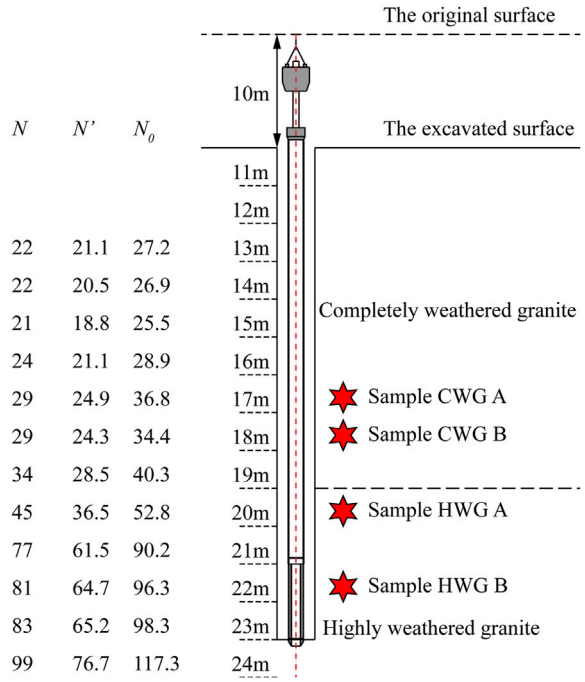

FIGURE 3 | SPT results and sample acquisition depth.

weathered granite is a typical soft rock in which the joint and fissure are well developed.

The research objects of this paper are CWG and HWG, which were got from stratum 2 and 3.

Sample Collection

It can be seen from **Section 2.1** that the weathered granite is loose and easy to be damaged, and its original structure would be easily destroyed during the sampling process of drilling (Xiong et al., 2022). In order to minimize disturbance, a sampling technique via hand-dug open pit (Zhang et al., 2017) was adopted to obtain the original block sample. Firstly, the ground was excavated to the desired depth. The weathered granites were cut into cuboids (side length approximates 300 mm) by the tools such as saws (as shown in **Figure 2A**), and then a stretch film was used to tie the samples to protect the sample (**Figure 2B**). The samples were truncated from the ground and the stretch film was used again to tie the samples firmly. Subsequently, multilayer wrap films were used to seal the sample so as to avoid moisture loss (**Figure 2C**). Finally, the sealed sample was put into the sample box and filled with pearl cotton around the inner wall of the sample box (**Figure 2D**), in order to fully reduce the disturbance of sample in the process of transportation.

The undisturbed samples were collected at a depth of 17–22 m from the original ground, as shown in **Figure 3**. The details of the samples were summarized in **Table 1**. In order to judge the weathering degree of the weathered granite, standard penetration tests (SPT) were conducted. The results of the standard penetration tests can reflect the strength and stiffness nature of geomaterial and are often used to judge the weathering degree of weathered granites (Chang and Zhang, 2018). Since the original ground was mountainous and hence the surface was uneven (as shown in **Figure 1**), SPT was uneasy to carry out. Therefore, the site was leveled, and the standard penetration test was carried out on the excavated ground surface. **Figure 3** presents SPT results from the borehole.

The SPT-N value got from the original ground surface is different from the that got from the excavated ground surface. According to the previous studies, different depths of geomaterials can be compared with each other by using the corrected SPT- N' value revised by the drill rod from the SPT- N value. Therefore, in this paper, the corrected N' value is used to compare the properties of weathered granite. The drill rod length correction coefficients are obtained from the China National Standard for Geotechnical Testing Method GB/T 50123 (2019) and the corrected SPT- N' values were also summarized in **Figure 3**. As shown in **Figure 3**, the SPT- N' value of weathered granite in study area is stable when the depth is 13–16 m. When the depth is more than 16 m, the SPT- N' value begins to increase with the depth and undergoes a sharp increase at 20 m. It shows that the weathering degree of weathered granite decreases gradually with the increase of depth, but it does not vary uniformly. According to Code for Investigation of Geotechnical Engineering GB 50021 (2001), the SPT- N_0 value obtained from the original surface was used to judge the weathering degree of granite. The SPT- N_0 value of CWG was less than 50 and the SPT- N_0 value of HWG was greater than 50. In this study, the SPT- N_0 value of the original ground surface is predicted based on the corrected SPT- N' value by the inverse calculation method for the rod length correction formula. The SPT- N_0 values are also summarized in **Figure 3**, which indicates

TABLE 1 | Parameters for weathered granite samples.

Samples	Abbreviations	Depth(m)	N value	N′ value
Completely weathered granite A	CWG A	17	29	24.9
Completely weathered granite B	CWG B	18	29	24.3
Highly weathered granite A	HWG A	20	45	36.5
Highly weathered granite B	HWG B	22	81	64.7

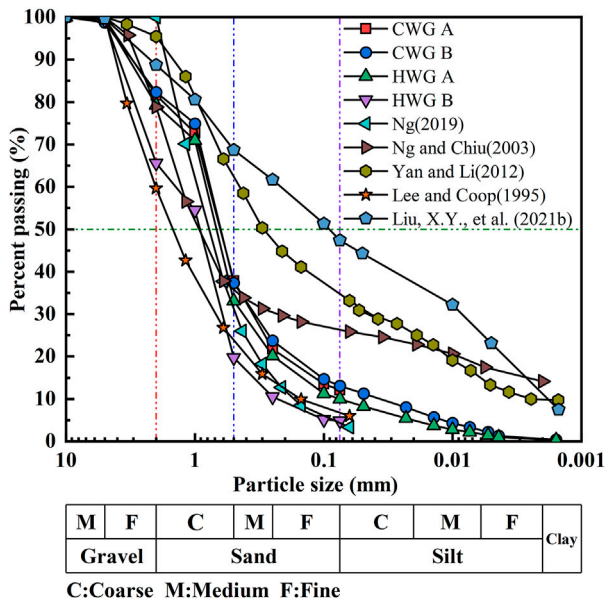

FIGURE 4 | Grain-size distribution curve of weathered granites (Data from Lee and Coop (1995); Ng and Chiu (2003); Yan and Li (2012); Ng et al. (2019); Liu X. et al. (2021).

that the boundary between CWG and HWG is a depth of 19 m for the test borehole.

Physical Characteristics

The index properties of weathered granites were studied by laboratory tests according to the China National Standard for Geotechnical Testing Method GB/T 50123 (2019). The grain size distribution analysis tests were conducted by the sieving method (for particle size≥0.075 mm) and the densimeter method (for particle size<0.075 mm), and four grain size distribution analysis test results were shown in **Figure 4**. It is observed that the maximum particle size of the studied samples is more than 5 mm, most of the particles are sand grains, followed by gravel, while the silt and clay contents occupy the lowest proportion. The coefficient of nonuniformity C_u is 6.2–15.7, and the coefficient of curvature C_c is 1.15–3.4, so the weathered granites in this study can be regarded as a coarse-grained but well-graded sand. Furthermore, it is apparent that the grain size distribution curve of the samples studied in this paper is close to that studied by Lee and Coop (1995) and Ng and Chiu (2003), but is located significantly below that studied by Yan and Li (2012) and Liu X. et al. (2021). The content of each particle size is summarized in **Table 2**. As shown in **Table 2**, the content of particles greater than 0.25 mm is 71.8–89.5%, which also indicates that the samples studied in this paper have a lower degree of weathering. According to Code for Investigation of Geotechnical Engineering GB 50021 (2001), the studied samples were categorized as coarse sand and gravelly sand. Grain size distribution curves of different samples studied in this paper are nearly parallel, and with the weathering degree increasing, the content of grain size less than 0.075 mm increases significantly, indicating that the weathering degree of granite increases with the decrease in depth, but the grain size decreases continuously.

According to the China National Standards GB/T 50123 (2019), the basic physical properties of weathered granite are measured, including specific gravity tests, Atterberg limit tests, initial void ratio, and hydrometer analysis. The test results together with sample parameters from other locations are shown in **Table 3**. Compared with the samples from Hong Kong (Ng and Chiu, 2003; Yan and Li, 2012), Seoul (Lee and Coop, 1995), and Shenzhen (Liu P. et al., 2021), the specific gravity of weathered granites in the Lincang area is significantly higher, which is similar to the sample from Xiamen (Liu X. et al., 2021). According to the standard, the plastic index of the particles

TABLE 2 | The mass fractions of weathered granites in the Lincang area.

Samples	Mass fraction (%)							
	Gravel-sized		Sand-sized					
	>5 mm	2~5 mm	1–2	0.5–1	0.25–0.5	0.1–0.25	0.075–0.1	<0.075 mm
CWG A	0.4	18.0	8.9	34.8	16.1	8.2	1.5	12.1
CWG B	1.3	16.4	7.4	37.6	13.6	9.0	1.6	13.1
HWG A	0.4	20.3	8.4	37.8	12.9	8.9	1.2	10.1
HWG B	0.7	33.7	11.1	34.8	9.2	5.4	0.3	4.8

TABLE 3 | Basic physical properties and mechanical indices of weathered granites (Date from Lee and Coop (1995); Ng and Chiu (2003); Yan and Li (2012); Liu P. et al. (2021); Liu X. et al. (2021))

Samples	G_s	ρ_d (kg/cm^3)	e_0	I_p	Classification	Location
CWG A	2.699	1.544	0.716	14.7	Coarse sand	Lincang
CWG B	2.688	1.575	0.670	14.8	Coarse sand	Lincang
HWG A	2.697	1.531	0.763	13.4	Coarse sand	Lincang
HWG B	2.723	1.786	0.516	16.4	Gravelly sand	Lincang
Lee and Coop (1995)		1.713	-	-	-	Seoul
Ng and Chiu (2003)	2.61	-	-	-	Gravelly sand	Hong Kong
Yan and Li (2012)	2.58	-	-	15.0	SC-CL	Hong Kong
Liu, et al. (2021a)	2.60	1.45		15.0	SC	Shenzhen
Liu, et al. (2021b)	2.72	1.81	1.045	27.9	SC	Xiamen

G_s, Specific gravity; ρ_d, Natural dry density; e_0, Initial void ratio; I_p, Plasticity index.

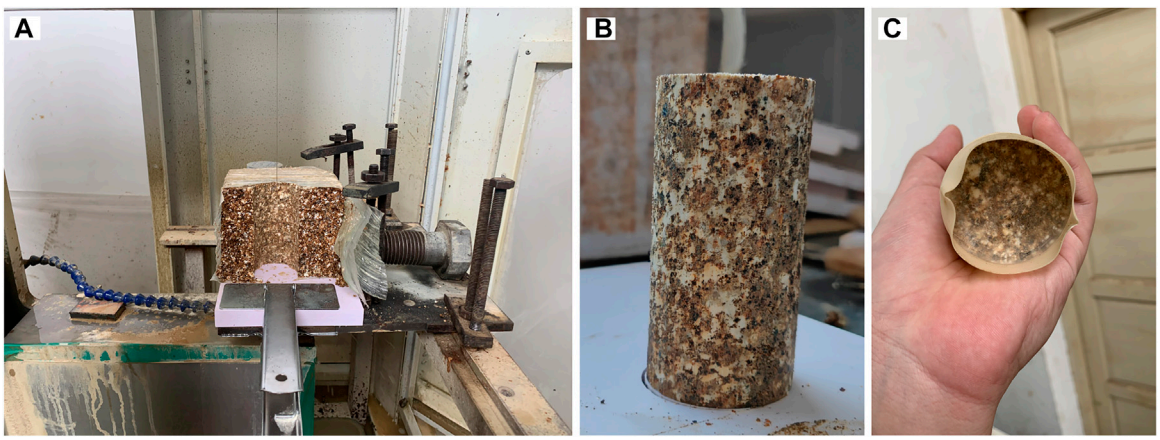

FIGURE 5 | Weathered granite samples processed by CNC abrasive wire sawing machine: **(A)** Circular CNC abrasive wire sawing machine; **(B)** Prepared sample; **(C)** Packaged sample.

less than 0.5 mm is 13.4–16.4, which further verifies that the research object in this paper has fewer fine grains and a lower weathering degree compared with others.

Specimen Preparation

It can be seen from **Figure 1**, **Figure 2** that the weathered granite in the Lincang area has a large particle size, in which the content of particle size above 0.25 mm is 71.8–89.5%, and has common characteristics of the weathered granite: loose structure, low interparticle cohesion and rapid disintegration in case of water (Liu et al., 2019). Meanwhile, the weathered granites are rich in brittle minerals such as quartz and unweathered feldspar, which results in the weathered granites having two characteristics: rigid particles and loose texture. Therefore, it is extremely difficult to make undisturbed samples of weathered granite by traditional sample preparation methods (Niu et al., 2014) such as cutting by knife. Through investigation and comparison of practice, this paper adopts a circular computer numerical control (CNC) abrasive wire sawing machine to treat weathered granites, as shown in **Figure 5A**. Li (2016) first applied the reciprocating abrasive wire cutting technology to the treat shale and coal rock samples and achieved satisfactory results. But compared with shale and coal rock, the inhomogeneity and fragility of weathered granites are more outstanding, which are easily broken without constraint outer pressure. The reciprocating abrasive wire cutting technology has two weaknesses in dealing with weathered granite as compared to the circular CNC abrasive wire sawing machine. There is an unavoidable difficulty that the line of reciprocating abrasive wire cutting machine is often broken in the process of cutting weathered granite samples. The explanation for this phenomenon might be that the content of minerals in weathered granites, such as quartz and unweathered feldspar, is higher and these minerals are not evenly distributed. In the meantime, the wire diameter (usually less than 0.35 mm) is small and the line needs to undergo reciprocating motion, so the sand line is easy to break due to the sudden increase of stress caused by quartz particles and feldspar particles in the cutting process. It is easy to damage the sample in the process of changing the monocrystalline wire. In addition, because the monocrystalline wire of the reciprocating abrasive wire cutting machine needs to repeat the reciprocating movement, and its line speed is not fast (less than 20 m/s),

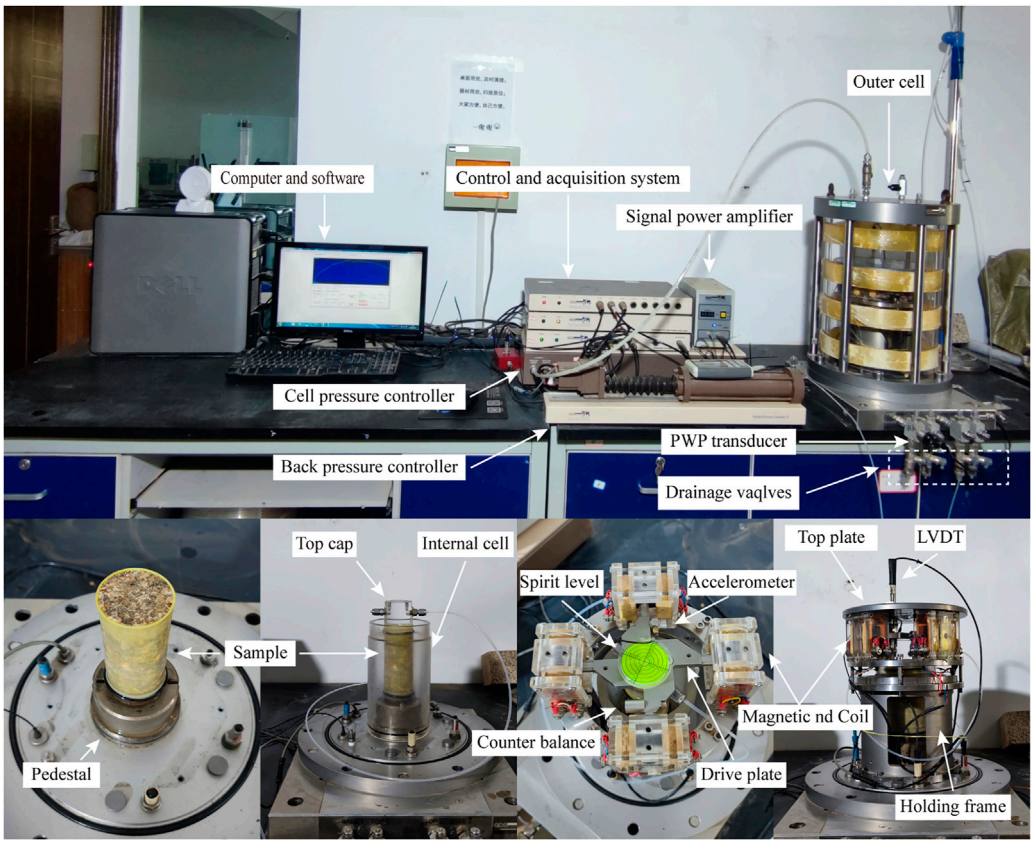

FIGURE 6 | Schematic view of the resonant-column apparatus and the experimental setup.

the efficiency of cutting weathered granites is lower. Relatively speaking, the circular CNC abrasive wire sawing machine (**Figure 5A**) adopted in this paper has a higher line speed (more than 40 m/s) due to the characteristics of the annular line without reciprocating movement. More importantly, the line diameter is thicker (diameter =0.65 mm), which is not easy to break in the cutting process, greatly improving the cutting efficiency and success rate of treating weathered granite. The obtained undisturbed sample (diameter d=50 mm; height h=100 mm) is shown in **Figure 5B**. It can be distinctly seen that the sample is unbroken and has a smooth surface, and the original structure of weathered granite can be seen clearly. The surface evenness of samples is acceptable, which can meet the test requirements.

After processed by the circular CNC abrasive wire sawing machine, the samples were directly encapsulated with a rubber membrane, and both ends of the weathered samples were fixed with plexiglass discs (as shown in **Figure 5C**). Constraint measures were also taken to prevent it from breaking during movement.

Before the resonance column test, the samples were placed in a water tank to be subject to vacuum pressure for 24 h. Then the initially saturated sample was installed on the experimental instrument and the back pressure was applied step by step to the sample in order to increase the saturation of the sample. The Skempton B value was checked until it was greater than 0.96, which can guarantee the saturation of the tested specimen. Then consolidation pressure was carried out. After the sample consolidation was completed, relevant tests were carried out.

TESTING EQUIPMENT AND TEST PROCEDURE

Testing Apparatus and Test Procedure

The tests in this study were performed with an automated resonance column testing system, which was manufactured by Global Digital Systems (GDS) Ltd. in the United Kingdom. The resonance column testing device was a Stokoe-type resonance column device, and the bottom end of the sample is fixed and the top end is free. The resonant column test system includes an excitation system, measuring system, and sample container (**Figure 6**). The resonance column testing apparatus was equipped with two pressure controllers (cell and back pressure), in addition to a LVDT displacement transducer to measure the axial strain. The volume and pressure accuracy of the backpressure control system are 1 mm^3 and

TABLE 4 | Experimental schemes of resonant column tests.

Samples	Consolidation pressure (kPa)	Backpressure (kPa)	Effective consolidation pressure (kPa)
CWG A CWG B HWG A HWG B	150, 200, 300, 400, 500, 600, 700, 800, 900, 1000	100	50, 100, 200, 300, 400, 500, 600, 700, 800, 900

1 kPa, respectively. The pressure accuracy of the cell pressure control system and pore water pressure transducer is 1 kPa. The accuracy of the axial displacement transducer is 0.001 mm which meets the accuracy requirement of the experiment. In the consolidated process, the backpressure was applied on the top cap, the pore water pressure was measured from the base of the specimen, and the volume change was measured via the back-pressure controller. The consolidation stage was considered complete when the drainage rate of pore water was less than 1 mm^3/min.

In the test process, the torsional excitation force was applied step by step at the free end of the specimen by controlling the excitation voltage of the excitation system, the specimen was vibrated by the torque at different frequencies and the corresponding shear strain of the sample was measured by the acceleration transducer (the representative shear strain is inferred from the rotation at a conventionally fixed radial distance). The frequency producing the maximum shear strain amplitude was considered as the resonant frequency. As the experiment proceeded, the intensity of the applied torque was increased step by step, which was controlled by the input voltage. The test stopped at the assigned consolidation pressure after loading approximately 20–25 levels of excitation force at each consolidation pressure. Therefore, the stiffness for increasing strain levels at each consolidation pressure could be determined.

The dynamic shear modulus G of the sample can be calculated by the following formula:

$$G = \rho(2\pi f H/\beta) \quad (1)$$

where G is the shear modulus of the sample, ρ is the density of the sample after consolidation, f is the resonance frequency, H is the height of the sample after consolidation, and β is the characteristic value of the frequency equation of torsional vibration, which can be obtained from the reference table.

Test Scheme

Since the strain range investigated in the resonance column test is less than 0.1%, it can be almost considered that there is no destruction to the sample during the resonance column test. Therefore, one sample can be used for the resonance column test at different consolidation pressures. The backpressure was all set for 100 kPa in all tests. To study the effects of effective consolidation pressure ($\sigma_m^{'}$), and weathering degree on the small strain stiffness properties of weathered granites, the specimens were investigated under various test conditions. The samples (CWG A, CWG B, HWG A, HWG B) were tested by the resonant column test at effective consolidation pressures of 50 kPa, 100 kPa, 200 kPa, 300 kPa, 400 kPa, 500 kPa, 600 kPa, 700 kPa, 800 kPa, 900 kPa. The specific test schemes are provided in **Table 4**.

RESULTS AND ANALYSIS

Effect of Effective Consolidation Pressure on Dynamic Shear Modulus

Results of the dynamic shear modulus G of all undisturbed samples at different effective consolidation pressures with shear strain γ are shown in **Figure 7**. According to the results in **Figure 7**, the relationship curves of dynamic shear modulus G and shear strain γ of weathered granite samples with different weathering degrees at different effective stresses are similar in shape and variation tendency. When the shear strain is small ($\gamma < 0.001\%$), the soil stiffness exhibits almost a fixed value. And when the shear strain exceeds 0.001%, it can be observed that the shear modulus becomes strain-dependent and the attenuation gradient of the dynamic shear modulus increases with the shear strain increasing. For the same sample, the phenomenon is more obvious under higher effective consolidated stresses. It indicates that with the increase in shear strain, the stress-strain relationship of weathered granite changes from linear to nonlinear, which is the characteristic of most geotechnical materials (Seed and Idriss, 1970; Stokoe et al., 1999).

In addition, one can see that curves of all samples move up with the increase of effective consolidation stress. In other words, dynamic shear modulus increased with the effective consolidation stress at the same shear strain. A similar phenomenon could be observed in sedimentary soil, sandy soil, and eluvial soil, which is obviously different from strongly structured soils. As the effective consolidation pressure increases, the structure of samples becomes denser. The contact area between particles increases and the propagation velocity of the shear wave is easier to accelerate in the sample. The resonance frequency measured in the test increases with the increase in consolidation pressure, so the maximum shear modulus increases with the increase in consolidation pressure. However, with the increase in consolidation pressure, the

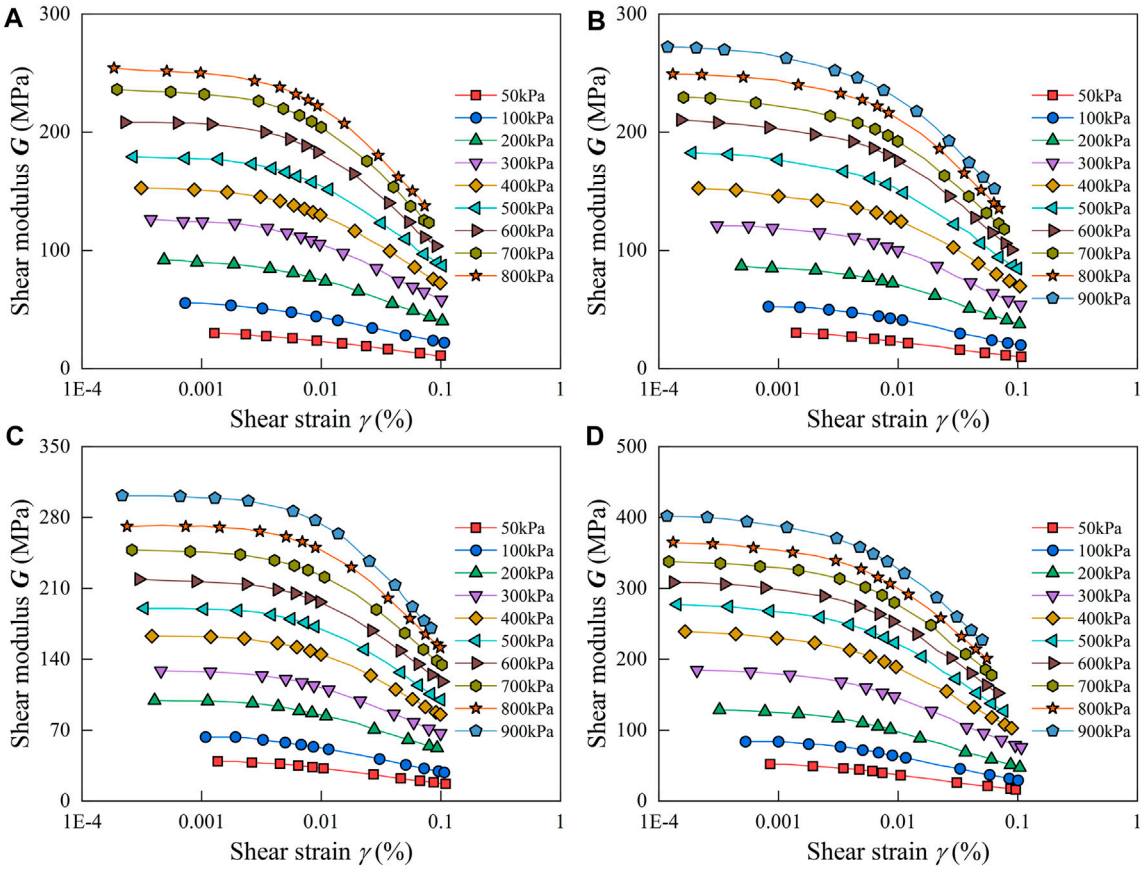

FIGURE 7 | Relationship between shear modulus *G* and shear strain γ for specimens in different weathering conditions: **(A)** CWG A; **(B)** CWG B; **(C)** HWG A; **(D)** HWG B (Data points halved).

volume of the sample decreases, and the increased amplitude of the maximum shear modulus gradually decreases.

Effect of Weathering Degree on Dynamic Shear Modulus

The variation of dynamic shear modulus *G* and shear strain γ of samples with different weathering degrees (corresponding different corrected SPT-N' value)under the same consolidation pressure are shown in **Figure 8**. One can see that the dynamic shear modulus curves of samples with different weathering degrees are significantly different at the same effective consolidation pressure. Samples with lower weathering degrees (higher corrected SPT-N' value) have higher shear modulus at the same shear strain, but the attenuation gradient of shear modulus is larger with the

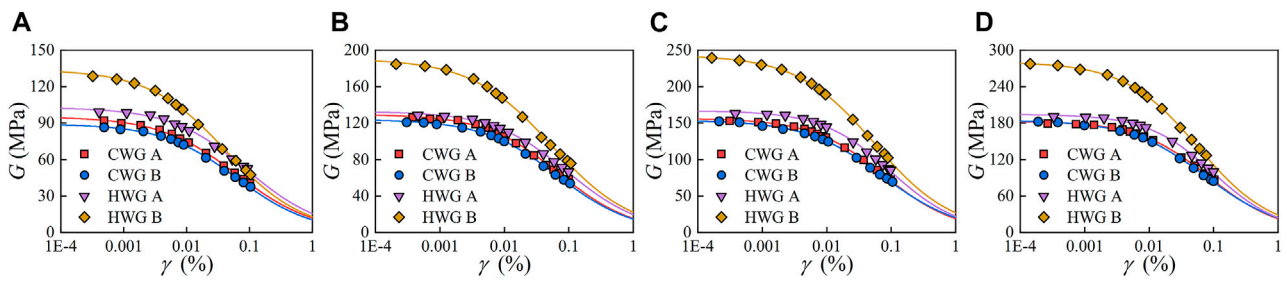

FIGURE 8 | Relationship between shear modulus *G* and shear strain γ for specimens at different effective consolidation pressures: **(A)** 200 kPa; **(B)** 300kPa; **(C)** 400kPa; **(D)** 500 kPa. (Data points halved).

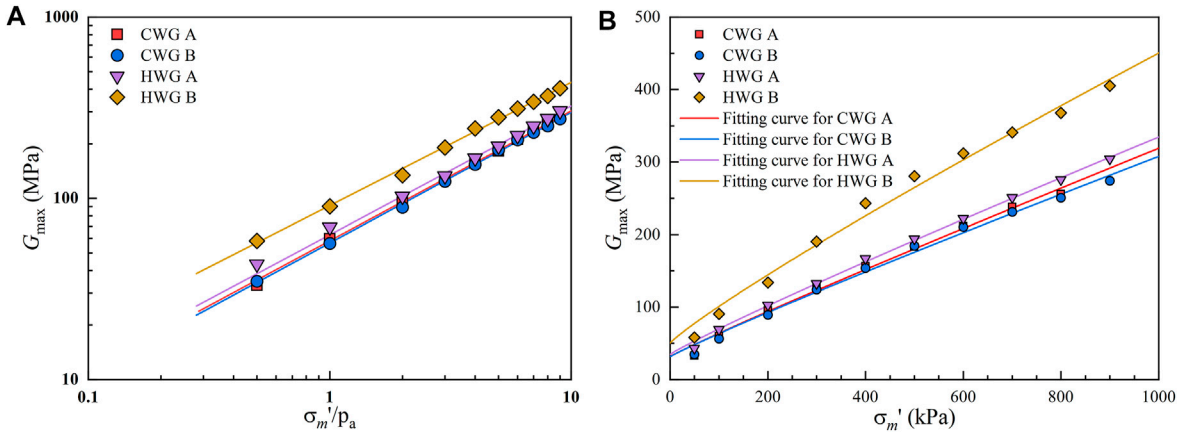

FIGURE 9 | G_{max} for specimens with different weathered degrees: **(A)** $G_{max} - \sigma_m'/p_a$; **(B)** $G_{max} - \sigma_m'$.

development of strain. This result may be explained by the fact that when granite weathering degree exceeds a threshold, fine particle content increases, the secondary cementation of the particle is becoming ever more obvious, which can delay the stiffness attenuation (Liu X. et al., 2021). The sample with a lower weathering degree has few fine particles, so the secondary cementation is lower than that of the sample with a higher weathering degree, which results in greater stiffness attenuation of the lower weathered sample.

Effect of Weathering Degree on Maximum Dynamic Shear Modulus

When the soil shear strain approximates the minimum, the corresponding dynamic shear modulus is defined as the maximum dynamic shear modulus G_{max}, which is an important parameter in the dynamic geotechnical analysis (Stokoe et al., 2005). The curve fitting between shear modulus G and shear strain γ is usually used to obtain the corresponding dynamic shear modulus. In this paper, the Stokoe formula (Stokoe et al., 1999), which was improved based on the Hardin-Drnevich equation, is used to fit the experimental results. The formula is described as follows:

$$G = \frac{G_{max}}{1 + (\gamma/\gamma_r)^c} \tag{2}$$

where γ_r is the reference shear strain when $G/G_{max} = 0.5$; c is the fitted curvature parameter. To improve the accuracy of the fitting curve, the method proposed by Yan et al. (2018) is adopted. The experimental data curves were first processed using the linear fitting, and the linear fitting parameters were used as nonlinear fitting input values to fit the experimental data curves again to obtain the final fitting parameters. The fitting curve is exhibited in **Figure 8**, from which it can be seen that the fitting curve are all highly consistent with the experimental data.

The relationship curves between the maximum dynamic shear modulus G_{max} of different weathered granites at different effective consolidation pressures are displayed in double logarithmic coordinates (**Figure 9A**). It can be observed that the maximum dynamic shear modulus G_{max} increases with the increase in effective consolidation pressure. The curves of samples with lower weathering degrees are higher than that with higher weathering degrees. As can be seen from **Figure 9A**. A highly significant linear relationship between the maximum dynamic shear modulus and effective consolidation stress was observed in the logarithmic coordinate for all samples and can be expressed by the common power function as follows.

$$G_{max} = G_0 \left(\frac{\sigma_m'}{P_a} \right)^n \tag{3}$$

where p_a is the atmospheric pressure ($p_a = 100\,kPa$ in this paper); σ_m' is the effective consolidation pressure; G_0 is the maximum shear modulus G_{max} when the effective consolidation pressure is 100 kPa; n is the fitting parameter, which is determined by experimental data. **Eq. 3** is similar to the famous Hardin formula, where n is the soil constant and affected by the type of soil and other factors. Observing the form of **Eq. 3**, it is easy to know that the maximum shear modulus G_{max} is 0 MPa when the effective consolidation pressure is 0 kPa, which does not fit with the actual situation. When the effective stress is 0 kPa, the maximum shear modulus of the soil is not 0 MPa. Therefore, **Eq. 3** is modified as follows.

$$G_{max} = G_0 \left(1 + \left(\frac{\sigma_m'}{P_a} \right)^n \right) \tag{4}$$

TABLE 5 | Summary of the G_{max} fitting parameters.

Samples	G_0	n	R^2	N'
CWG A	31.97	0.9534	0.991	24.9
CWG B	31.76	0.9393	0.991	24.3
HWG A	35.01	0.9324	0.998	36.5
HWG B	50.47	0.8991	0.989	64.7

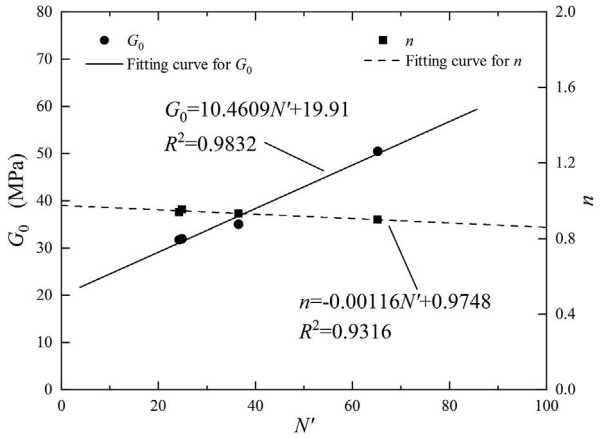

FIGURE 10 | G_0 and n for specimens with different SPT- N' value (different weathered degrees).

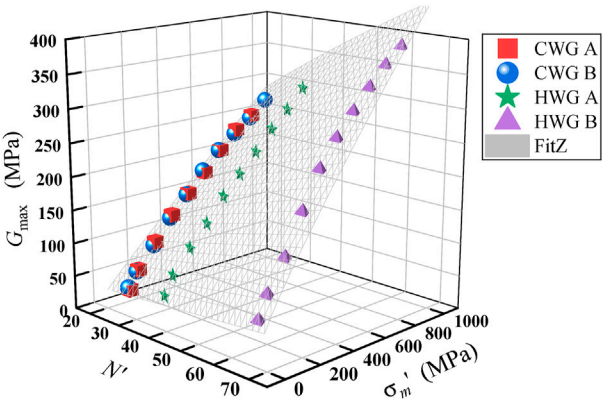

FIGURE 11 | Relationship of N', σ_m' and G_{max} for weathered granite in the Lincang area.

where G_0 is the maximum shear modulus G_{max} when the effective consolidation pressure is 0 kPa. The modified equation satisfies the case where the effective stress is 0 kPa, and as the effective stress increases, it is a monotonic function and gradually converges towards **Eq. 3**.

The fitting parameters of the maximum dynamic shear modulus G_{max} with different weathering degrees are shown in **Table 4** and the fitting curves of the test data are shown in (**Figure 9B**). **Table 5** shows that the fitting parameter G_0 and n variation with different weathering degrees, for which the minimum R^2 is 0.989, indicating a good fit. G_0 shows an increase in value with decreasing weathering degree and n shows an increase in value with increasing weathering degree. The n value reflects that the sample with a higher weathering degree is more sensitive to the change of effective consolidation pressure, which has a higher n value. This phenomenon may be explained by the fact that the sample with a higher weathering degree has smaller dry density and larger porosity, the skeleton of which is easier to be compressed at consolidation pressure.

According to the relationship between the fitted parameters and the SPT- N' values in **Table 5**, the parameters G_0, n, and SPT- N' values have a good linear relationship, as shown in **Figure 10**. Substituting the fitted equations for the parameters G_0 and n in **Figure 10** into **Eq. 4**, the characterization of the maximum dynamic shear modulus considering the degree of weathering is obtained. **Eq. 4** can be rewritten in

$$G_{max} = \left(A \times N' + B\right)\left(1 + \left(\frac{\sigma_m'}{p_a}\right)^{C \times N' + D}\right) \quad (5)$$

where A and B are the fitting parameters for G_0, C and D are the fitting parameters for n, and P_a is the atmospheric pressure (P_a = 100 kPa in this paper).

Based on regression analysis using the least square method shown in **Figure 10**, the following expression was derived for the model parameter of weathered granites in the Lincang area:

$$G_{max} = \left(0.46092N' + 19.91\right)\left(1 + \left(\frac{\sigma_m'}{p_a}\right)^{-0.00116N' + 0.9748}\right) \quad (6)$$

Figure 11 gives the test results and Fitting surface in terms of a three-dimensional plot. The data analysis in **Figure 11** showed a strong correlation between the maximum shear modulus (G_{max}) of the tests and the maximum shear modulus (G_{max}) calculated by the effective consolidation pressure (σ_m') and the corrected SPT N' value (N') (R^2 equal to 0.989). **Formula (6)** can be directly used to calculate the maximum dynamic shear modulus of the weathered granites in the Lincang area under the condition of isotropic consolidation by the N' value obtained from the in-situ test.

Attenuation Characteristics of the Dynamic Shear Modulus

The dynamic shear modulus ratio, which reflects attenuation characteristics of the dynamic shear modulus with the development of dynamic strain, is the key input parameter in the process of soil dynamic analysis. For the convenience of analysis, the test data are normalized with the maximum dynamic shear modulus. Changing the form of **Eq. 2** gives the following relationship, which can be used to fit the corresponding data.

$$\frac{G}{G_{max}} = \frac{1}{1 + \left(\gamma/\gamma_r\right)^c} \quad (7)$$

Figure 12 shows the results of the dynamic shear modulus ratio. Some fitting parameters are shown in **Table 6**. It can be seen that the reference shear strains γ_r and the fitted curvature parameter c of all samples increases with the increase in consolidation pressure, indicating that the stiffness attenuation gradient of all samples decreases with the increase in consolidation pressure. This phenomenon can be explained that with the increase in consolidation pressure, the pore ratio of samples decreases and the particles in the sample contact more closely and the intergranular force is larger, and the resistance to deformation is strengthened. Therefore, the samples are more

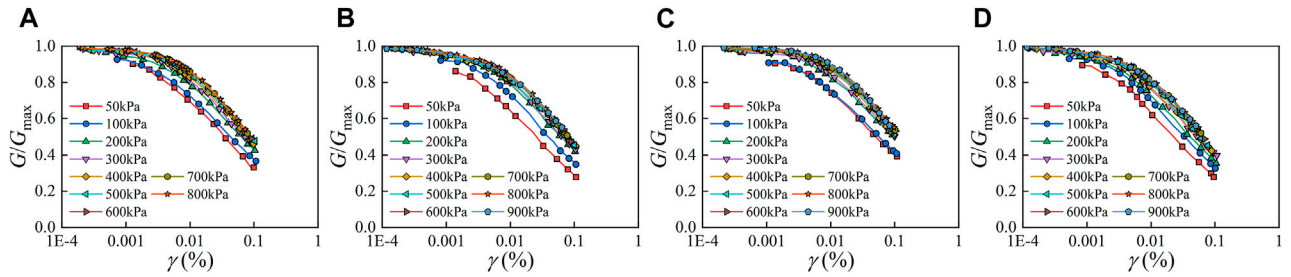

FIGURE 12 | Normalized stiffness $G/G_{max} - \gamma$ attenuation curves for specimens with different weathering degrees: **(A)** CWG A;**(B)** CWG B;**(C)** HWG A; **(D)** HWG B (Data points halved).

TABLE 6 | Fitting parameters of test data of samples with varying weathering degrees.

Samples	50 kPa		100 kPa		200 kPa		400 kPa		800 kPa	
	γ_r	c	γ_r	c	γ_r	c	γ_r	c	γ_r	c
CWG A	0.0345	0.6761	0.0443	0.6547	0.0636	0.7059	0.0777	0.7728	0.0858	0.8549
CWG B	0.0256	0.6616	0.0422	0.7163	0.06361	0.7325	0.0751	0.7262	0.0835	0.7952
HWG A	0.0529	0.6601	0.0578	0.6458	0.0911	0.7211	0.0991	0.8119	0.1183	0.8661
HWG B	0.0235	0.6857	0.0344	0.7038	0.0428	0.7067	0.0557	0.7213	0.0687	0.7771

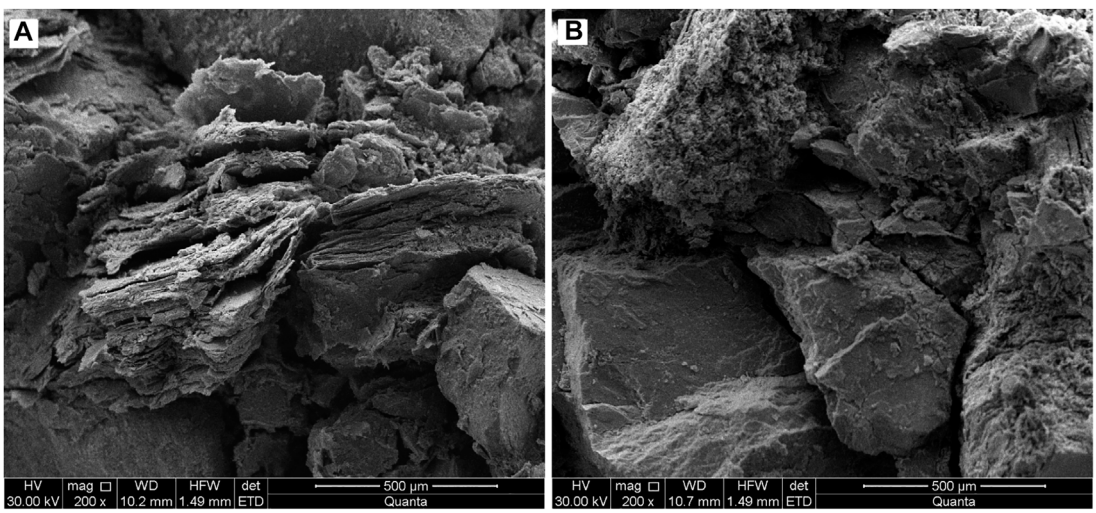

FIGURE 13 | SEM micrographs of HWG B in a vertical plane of specimen under 200x magnification: **(A)** the natural state; **(B)** at an effective consolidation pressure of 900 kPa.

resistant to deformation, the dynamic shear modulus of which can be maintained at a larger shear strain amplitude.

DISCUSSION

The Variations of Small Strain Stiffness Properties in the View of the Microstructure

To observe the effect of consolidation pressure on the micro-morphological changes of weathered granite, the weathered granite was treated with a heating and drying method in advance. Experimental analysis of the treated HWG B using scanning electron microscopy (SEM) and SEM images are shown in **Figure 13**. As shown in **Figure 13A**, the structure of the undisturbed HWG is an interlocking structure. The mineral particles are uneven in size, with some small particles filling in between the larger ones, and the particles have an angular and irregular shape. The distribution of fractures between the particles is obvious, and the width of fractures is large. The pore type is mainly intergranular pores, the primary fissures and their development direction is irregular, and most of the fissures penetrate each other, and the minerals cannot be observed in some fissures, indicating that

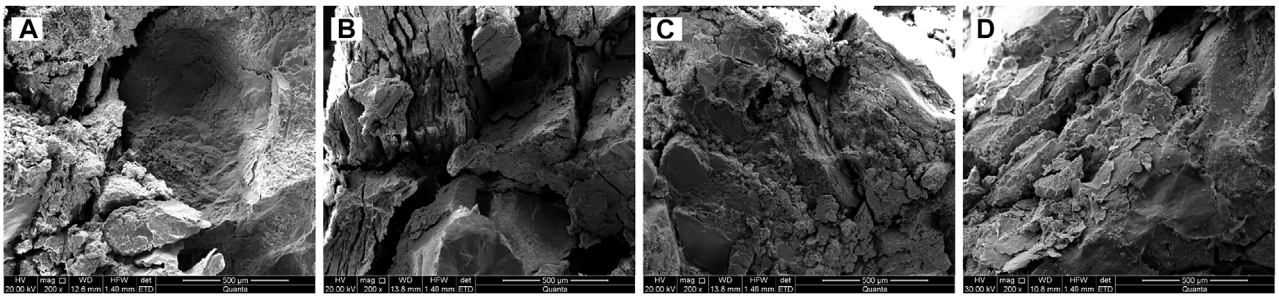

FIGURE 14 | SEM micrographs of the weathered granites at the natural state in a vertical plane for specimens in different weathering conditions under 200x magnification: **(A)** CWG A; **(B)** CWG B; **(C)** HWG A; **(D)** HWG B.

the fissure depth is large and the gap between the particles is large and that the weathered granite structure is loose. There is almost no cementing material between the particles, but the shapes of adjacent particles match each other, indicating that the interparticle fissures should be attributed to the loss of weathered minerals. It is noteworthy that there are flakes of highly weathered protolithic minerals between some of the quartz grains, and the flake structure is layered in face-to-face contact with obvious relaxation of the lamellar structure and large internal spacing. As can be seen from **Figure 13B**, the structure of the undisturbed HWG after consolidation becomes denser, the fissures between the particles are closed, and the fissures of the original laminated structure inside some particles are tightly closed due to the consolidation pressure. In summary, the undisturbed HWG after consolidation are more compaction in structure, which makes the shear wave propagate faster in the sample, and therefore the shear modulus of the sample increases.

The soil structure of unconsolidated weathered granites with different weathering degrees was investigated using SEM, and the SEM images are shown in **Figure 14**. SEM photographs show that the structural fragmentation of the weathered granite increases with the increase of weathering degree. As the degree of particle fragmentation increases, the number of fine particles increases, the fine particles attached to large particles also increase, and the angles of some particles gradually tend to be round with the increase in weathering degree. The fracture spacing between large particles increases and some of the fractures in the samples with a higher weathering degree are filled with small particles. Tiny fractures increase in some of the particles themselves. To summarize, with the increase in weathering degree, the fine particles increase, the fissures are more developed and the shear wave propagation is more difficult, which is the reason for the decrease of shear modulus.

Recommended Range of Small Strain Stiffness Parameters for Weathered Granite in the Lincang Area

In order to provide parameter suggestions for the dynamic analysis of weathered granite stratum engineering construction in the Lincang area, this paper sorted out the experimental results and presented the variation range of stiffness parameters of weathered granite in the Lincang area, as shown in **Figure 15**. In order to facilitate comparative analyses, the results of other geomaterials were also put in the figure. It can be seen from **Figure 15** that for weathered granite with different weathering degrees, the decay curve of dynamic shear modulus shows the same change trend, but there are some differences in the attenuation rate. The previous results have indicated that the sample with a higher weathering degree is more sensitive to the effective stress, but the samples with a lower weathering degree are more susceptible to the shear strain, and hence the attenuation rate is faster. The small strain (10^{-6}–10^{-3}) test of the resonant column shows that the weathered granites have basically identical dynamic response and regularity to the usual sand samples (Zhu and Xu, 1993; Yuan et al., 2000). The attenuation rate of the dynamic shear modulus ratio of the weathered granites in the Lincang area with increasing dynamic shear strain is basically lower than the upper boundary attenuation rate of the general sand curve, which was suggested by Seed and Idriss (1970). According to the modulus ratio data points, when the shear strain is 10^{-6}–10^{-4}, all weathered granites data points are distributed above the lower

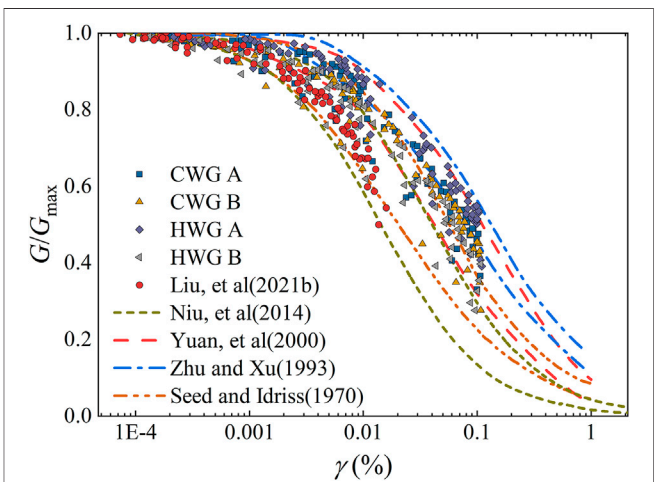

FIGURE 15 | Results of normalized dynamic shear modulus. Data source: Seed and Idriss (1970); Zhu and Xu (1993); Yuan et al. (2000); Niu et al. (2014); Liu X. et al. (2021).

boundary of the remolded HWG curve reported by Niu et al. (2014), and some data points are outside the upper boundary of the reconstituted high weathered curve suggested by (Niu et al., 2014). Furthermore, all data points of the weathered granites in the Lincang area are distributed under the upper boundary of the sand curve suggested by Yuan et al. (2000). As can be seen from **Figure 15**, the lower limit of sand soil range given by Yuan et al. (2000) almost coincides with the upper limit of reconstituted HWG range given by Niu et al. (2014), the results range of Lincang granite is the area where the two ranges merge. In addition, the experimental results range of granite residual soil studied by Liu X. et al. (2021) are consistent with that of reconstituted HWG provided by Niu et al. (2014). As the strain increases ($>10^{-4}$), the range of weathered granites data in the Lincang area gradually changes to almost cover the range of sand given by Zhu and Xu (1993) and Yuan et al. (2000), and has little overlap with the range given by Niu et al. (2014), indicating that the attenuation curves of dynamic shear modulus ratio of weathered granite in different areas have obvious differences. Although the decay trend of the dynamic shear modulus ratio of weathered granite in different regions is the same, the attenuation rate does differ significantly. There will be an obvious deviation in the dynamic analysis of the Lincang area if the experimental results of other areas are forcibly applied. In summary, compared to the data provided by Niu et al. (2014) and Liu X. et al. (2021), the weathered granites in the Lincang area exhibit the shear modulus ratio that decreases at a smaller rate with the development of dynamic shear strain and a broader variation range. Thus, the weathered granites in Lincang area are more resistant to deformation than that in other areas and suitable for serving as a construction material.

CONCLUSION

In this paper, a series of resonance column tests were carried out on undisturbed completely and highly weathered granite in the Lincang area to study its dynamic shear modulus characteristics, and the results were compared with those of others. The main conclusions and results obtained are as follows:

1) The *via* hand-dug open pit method was used to obtain undisturbed block weathered granite samples with minimal disturbance. A circular CNC abrasive wire sawing machine has a good processing effect on weathered granites which have rigid particles and loose texture and may be extended to the treatment of other undisturbed rock and soil materials.
2) The Stokoe formula provides a good fit to the curve of $G - \gamma$ for weathered granite in the Lincang area. At the same strain level, the maximum dynamic shear modulus of weathered granite increases with the increase in effective consolidation pressure but decreases with the increase in weathering degree. The maximum dynamic shear modulus of weathered granite with a higher weathering degree is more sensitive to the effective consolidation pressure. The fitting curve for the maximum dynamic shear modulus was given, and the fitting parameters G_0 and n have a good linear relationship with SPT- N' values.
3) The fitting formula and related parameters of the dynamic shear modulus of Lincang weathered granite were proposed, and the variation range of dynamic parameters was given. The attenuation rate of dynamic shear modulus ratio of weathered granite in the Lincang area with shear strain is significantly lower than that in other areas, indicating that dynamic parameters of weathered granite samples in different areas vary in different ranges. The parameters suggested in this paper can provide a basis for dynamic stability analysis of weathered granite stratum engineering construction.

DATA AVAILABILITY STATEMENT

The original contributions presented in the study are included in the article/Supplementary Material, further inquiries can be directed to the corresponding author.

AUTHOR CONTRIBUTIONS

JW wrote the manuscript. JW and CL conducted the in-situ test and collected the samples. JW prepared the sample of the laboratory test. JW and JY conducted the resonance column test. LK and BL wrote and edited the manuscript.

FUNDING

The research reported in this manuscript is funded by the Natural Science Foundation of China (Grants No. 11672320).

REFERENCES

Burland, J. B., Rampello, S., Georgiannou, V. N., and Calabresi, G. (1996). A Laboratory Study of the Strength of Four Stiff Clays. *Géotechnique* 46 (3), 491–514. doi:10.1680/geot.1996.46.3.491

Chang, S. B., and Zhang, S. M. (2018). *Geotechnical Engineering Handbook*. the fifth edition. Beijing, China: ChinaBuilding Industry Press.

Cui, Q.-L., Wu, H.-N., Shen, S.-L., and Xu, Y.-S. (2016). Geological Difficulties and Countermeasures for Socket Diaphragm Walls in Weathered Granite in Shenzhen, China. *Bull. Eng. Geol. Environ.* 75 (1), 263–273. doi:10.1007/s10064-015-0740-y

GB 50021 (2001). *Ministry of Housing and Urban-Rural Construction of the People's Republic of China*. Beijing. China. (in Chinese).(Code for Investigation of Geotechnical Engineering

GB/T 50123 (2019). *The China National Standards.Ministry of Housing and Urban-Rural Construction of the People's Republic of China*. Beijing. China. (in Chinese).

Huang, X., Cai, X., Bo, J., Li, S., and Qi, W. (2021). Experimental Study of the Influence of Gradation on the Dynamic Properties of Centerline Tailings Sand. *Soil Dyn. Earthq. Eng.* 151, 106993. doi:10.1016/j.soildyn.2021.106993

Irfan, T. Y., and Dearman, W. R. (1978). Engineering Classification and Index Properties of a Weathered Granite. *Bull. Int. Assoc. Eng. Geol.* 17 (1), 79–90. doi:10.1007/bf02634696

Irfan, T. Y. (1996). Mineralogy, Fabric Properties and Classification of Weathered Granites in Hong Kong. *Q. J. Eng. Geol. Hydrogeology* 29, 5–35. doi:10.1144/gsl.Qjegh.1996.029.P1.02

Kong, L., Zang, M., and Guo, A. (2017). Structural Damage Effect on Dynamic Shear Modulus of Zhanjiang Clay and Quantitative Characterization. *Chin. J. Geotechnical Eng.* 39 (12), 2149–2157.

Lee, C. (1965). *The Geotechnical Properties of a Decomposed Granite*. London: University of London.

Lee, I. K., and Coop, M. R. (1995). The Intrinsic Behaviour of a Decomposed Granite Soil. *Géotechnique* 45 (1), 117–130. doi:10.1680/geot.1995.45.1.117

Li, C., Kong, L., Shu, R., An, R., and Jia, H. (2020). Dynamic Three-Dimensional Imaging and Digital Volume Correlation Analysis to Quantify Shear Bands in grus. *Mech. Mater.* 151, 103646. doi:10.1016/j.mechmat.2020.103646

Li, J., Kong, L., and Jin, L. (2021). Stress History and Time Effect on Shear Modulus of Expansive Soils. *Arab. J. Geosci.* 15 (1), 35. doi:10.1007/s12517-021-09342-y

Li, X. (1996). Basic Characteristics and Formation Structural Environment of Lincang Composite Granite Batholith. *Yunnan Geol.* 15, 18.

Li, X. (2016). *Rock Physical Experiment and Fracturing Potential Characterization of Shale Gas Reservoir*. Xi'an: Northwest University.

Liu, J., Chen, W., Nie, W., Yuan, J., and Dong, J. (2019). Experimental Research on the Mass Transfer and Flow Properties of Water Inrush in Completely Weathered Granite under Different Particle Size Distributions. *Rock Mech. Rock Eng.* 52 (7), 2141–2153. doi:10.1007/s00603-018-1719-3

Liu, P., Yang, X. Q., and Zhou, X. W. (2021a). Mechanics of Completely Decomposed Granite: Example of Transitional Behavior. *Int. J. Geomechanics* 21 (9), 6. doi:10.1061/(asce)gm.1943-5622.0002142

Liu, X., Zhang, X., Kong, L., Li, X., and Wang, G. (2021b). Effect of Cementation on the Small-Strain Stiffness of Granite Residual Soil. *Soils Found.* 61 (2), 520–532. doi:10.1016/j.sandf.2021.02.001

Macari, E. J., and Hoyos, L. (1996). Effect of Degree of Weathering on Dynamic Properties of Residual Soils. *J. Geotech. Engrg.* 122 (12), 988–997. doi:10.1061/(asce)0733-9410(1996)122:12(988)

Ng, C. W. W., Akinniyi, D. B., Zhou, C., and Chiu, C. F. (2019). Comparisons of Weathered Lateritic, Granitic and Volcanic Soils: Compressibility and Shear Strength. *Eng. Geol.* 249, 235–240. doi:10.1016/j.enggeo.2018.12.029

Ng, C. W. W., and Chiu, A. C. F. (2003). Laboratory Study of Loose Saturated and Unsaturated Decomposed Granitic Soil. *J. Geotech. Geoenviron. Eng.* 129 (6), 550–559. doi:10.1061/(asce)1090-0241(2003)129:6(550)

Ng, C. W. W., and Wang, Y. (2001). Field and Laboratory Measurements of Small Strain Stiffness of Decomposed Granites. *Soils Found.* 41 (3), 57–71. doi:10.3208/sandf.41.3_57

Ng, C. W. W., and Yung, S. Y. (2008). Determination of the Anisotropic Shear Stiffness of an Unsaturated Decomposed Soil. *Géotechnique* 58 (1), 23–35. doi:10.1680/geot.2008.58.1.23

Niu, L., Song, Q. J., Xu, S., and Guo, X. M. (2014). "Dynamic Experimental Study on Highly Weathered Granite," in International Conference on Experimental and Applied Mechanics (EAM), DURNTEN-ZURICH (Tanjin: Trans Tech Publications Ltd), 132–137. doi:10.4028/www.scientific.net/AMM.518.132

Niu, X., Sun, Y., Yao, Y., and Han, J. (2015). Basic Properties and Weathering Process of Strong Weathered Granite. *JGS Spec. Publ.* 1 (2), 28–33. doi:10.3208/jgssp.CPN-07

Quan, F., Zhao, Y., Zhao, C. J., and Gao, M. C. (2021). Treatment Technology of Dissolution Fissure and Pipeline Type Water Inrush and Mud Inrush in Granite Formation. *Inn. Mong. Sci. TEchnology&Economy* 476 (10), 100–106.

Seed, H. B., and Idriss, I. M. (1970). *Report EERC 70-10, Earthquake Engineering Research Center*. Berkeley: University of California.Soil Moduli and Damping Factors for Dynamic Response Analyses

Shang, Y., Yue, Z., Park, H.-D., and Hyun, C.-U. (2015). Brittle Fracture and Plastic Creep of the Completely Decomposed Granite Presented in CT. *Geosystem Eng.* 18 (6), 338–347. doi:10.1080/12269328.2015.1075438

Stokoe, K. H., Darendeli, M. B., Andrus, R. D., and Brown, L. T. (1999). "Dynamic Soil Properties: Laboratory, Field and Correlation Studies," in 2nd International Conference on Earthquake Geotechnical Engineering (LEIDEN: A a Balkema Publishers), 811–845.

Stokoe, K. H., Rathje, E. A., and Axtell, P. J. (2005). "Development of an *In Situ* Method to Measure the Nonlinear Shear Modulus of Soil," in 16th International Conference on Soil Mechanics and Geotechnical Engineering (ROTTERDAM: Millpress Science Publishers), 751–754. Millpress.

Wang, K., Li, S., Yang, L., Zhang, Q., Li, Z., Qi, Y., et al. (2016). Study and Application of Full-Section Curtain Grouting after Disaster on Strongly Disturbed and Completely Decomposed Granite Formation. *dtetr*, 179–184. doi:10.12783/dtetr/emme2016/9811

Xiong, X., Xiong, Y., Okino, S., Mikami, R., Ma, J., and Zhang, F. (2022). Element Tests on the Hydraulic/mechanical Behaviour of Unsaturated Decomposed Granite Soil under Various Conditions. *Bull. Eng. Geol. Environ.* 81 (1), 15. doi:10.1007/s10064-021-02495-w

Yan, W. M., and Li, X. S. (2012). Mechanical Response of a Medium-Fine-Grained Decomposed Granite in Hong Kong. *Eng. Geol.* 129-130, 1–8. doi:10.1016/j.enggeo.2011.12.013

Yan, Z., Chen, X., Gao, Z., Yang, W., and Hong, H. (2018). Study on Nonlinear Fitting Results of Resonant Column Test. *China Earthq. Eng. J.* 40 (5), 1124–1130.

Yi, G., Fu, H., Wang, S., Wen, X., and Long, F. (2014). Analysis on Stress State in Seismogenic Area before Lancang-Gengma M7. 6 and M7.2 Earthquakes in 1988. *J. Seismol. Res.* 37 (3), 332–338.

Yuan, X., Sun, R., Sun, J., Meng, S. J., and Shi, Z. J. (2000). Laboratory Experimental Study on Dynamic Shear Modulus Ratio and Damping Ratio of Soils. Earthquake Engineering and Engineering Vibration.

Zhang, S., Liu, Y., Bate, B., Peng, D.-l., Li, C., and Zhan, L.-t. (2021). Quantitative Human Risk Analysis of 2015 Shenzhen Dump Failure Considering Influence of Urbanization. *J. Mt. Sci.* 18 (6), 1439–1457. doi:10.1007/s11629-020-6260-7

Zhang, X. W., Kong, L. W., Yin, S., and Chen, C. (2017). Engineering Geology of Basaltic Residual Soil in Leiqiong, Southern China. *Eng. Geol.* 220, 196–207. doi:10.1016/j.enggeo.2017.02.002

Zhu, L., and Xu, C. (1993). The Resonant Column Device and its Application in Engineering. *Dam Observation Geotechnical Tests* 17, 32–37

Conflict of Interest: The authors declare that the research was conducted in the absence of any commercial or financial relationships that could be construed as a potential conflict of interest.

Publisher's Note: All claims expressed in this article are solely those of the authors and do not necessarily represent those of their affiliated organizations, or those of the publisher, the editors and the reviewers. Any product that may be evaluated in this article, or claim that may be made by its manufacturer, is not guaranteed or endorsed by the publisher.

Copyright © 2022 Wang, Kong, Li, Liu and Yan. This is an open-access article distributed under the terms of the Creative Commons Attribution License (CC BY). The use, distribution or reproduction in other forums is permitted, provided the original author(s) and the copyright owner(s) are credited and that the original publication in this journal is cited, in accordance with accepted academic practice. No use, distribution or reproduction is permitted which does not comply with these terms.